DEVELOPMENTAL DYNAMICS 240:1586–1599, 2011

Fgfr3 Regulates Development of the Caudal Telencephalon

Randal X. Moldrich,[1] Cecilia Mezzera,[2] William M. Holmes,[3] Sailaja Goda,[4] Sam J. Brookfield,[4] Alastair J. Rankin,[4] Emily Barr,[4] Nyoman Kurniawan,[5] Deborah Dewar,[3] Linda J. Richards,[1,6] Guillermina López-Bendito,[2] and Tomoko Iwata[4]*

The fibroblast growth factor receptor 3 (Fgfr3) is expressed in a rostral$_{low}$ to caudal$_{high}$ gradient in the developing cerebral cortex. Therefore, we hypothesized that Fgfr3 contributes to the correct morphology and connectivity of the caudal cortex. Overall, the forebrain structures appeared normal in *Fgfr3*$^{-/-}$ mice. However, cortical and hippocampal volumes were reduced by 26.7% and 16.3%, respectively. Hypoplasia was particularly evident in the caudo-ventral region of the telencephalon where proliferation was mildly decreased at embryonic day 18.5. Dysplasia of GABAergic neurons in the amygdala and piriform cortex was seen following GAD67 immunohistochemistry. Dye-tracing studies and diffusion magnetic resonance imaging and tractography detected a subtle thalamocortical tract deficit, and significant decreases in the stria terminalis and lateral arms of the anterior commissure. These results indicate the subtle role of Fgfr3 in formation of caudal regions of the telencephalon affecting some brain projections. *Developmental Dynamics 240:1586–1599, 2011.* © 2011 Wiley-Liss, Inc.

Key words: Fgf; mouse; commissures; cortical volume; neurogenesis

Accepted 18 March 2011

INTRODUCTION

Fibroblast growth factors (Fgfs) are known to play various roles in the control of cellular differentiation, proliferation, migration, and axon guidance in the developing nervous system (Mason, 2007; Iwata and Hevner, 2009). There are 22 mammalian Fgf family members and four high-affinity tyrosine kinase receptors (Fgfr1–4) that mediate the majority of Fgf signaling with different binding affinities. In addition, heparan sulfate proteoglycans act as modifiers of Fgf ligand-receptor binding (Turner and Grose, 2010; Iwata and Hevner, 2009). All four Fgfrs are expressed in regions of the developing mouse brain and are likely to play roles in cellular proliferation, differentiation, and migration (Mason, 2007; Iwata and Hevner, 2009). Structural changes caused by altered Fgf signaling during embryonic development have been shown to influence cortical function and animal behavior (Cholfin and Rubenstein, 2008; Scearce-Levie et al., 2008). Therefore, it is important to identify the mechanism by which Fgfs regulate these processes.

One of the high-affinity Fgfrs, Fgfr3, is uniquely expressed in a rostro-caudal gradient, rostro-medial$_{low}$ to caudo-lateral$_{high}$, within the proliferative zones of the neocortex, septum, and lateral and medial ganglionic eminences (Fukuchi-Shimogori and Grove, 2003; Iwata and Hevner, 2009). A number of studies have been undertaken to dissect the relative contribution of Fgfrs to Fgf signaling in the developing telencephalon. Fgf signaling is necessary to

[1]The University of Queensland, Queensland Brain Institute, Brisbane, Australia
[2]Instituto de Neurociencias de Alicante, CSIC and Universidad Miguel Hernández, San't Joan d'Alacant, Spain
[3]Institute of Neuroscience and Psychology, College of Medical Veterinary and Life Sciences, University of Glasgow, Glasgow, United Kingdom
[4]School of Medicine, College of Medical Veterinary and Life Sciences, University of Glasgow, Glasgow, United Kingdom
[5]The University of Queensland, The Centre for Advanced Imaging, Brisbane, Australia
[6]The University of Queensland, The School of Biomedical Sciences, Brisbane, Australia
Grant sponsor: Neuroscience Foundation, Glasgow; Grant sponsor: National Health and Medical Research Council (NHMRC) Australia project; Grant number: 631552; Grant sponsor: Spanish Ministry of Science and Innovation; Grant numbers: BFU2009-08261, CONSOLIDER CSD2007-00023.
***Correspondence to: Tomoko Iwata, School of Medicine, MVLS, University of Glasgow, Beatson Institute for Cancer Research, Garscube Estate, Switchback Road, Bearsden, Glasgow, G61 1BD, UK. E-mail: Tomoko.Iwata@Glasgow.ac.uk**

DOI 10.1002/dvdy.22636
Published online 12 April 2011 in Wiley Online Library (wileyonlinelibrary.com).

© 2011 Wiley-Liss, Inc.

Developmental Dynamics

maintain the normal size of the telencephalon and it appears that each Fgfr plays an overlapping but individual role (Paek et al., 2009). The simultaneous deletion of Fgfr1 and Fgfr3, or Fgfr1 and Fgfr2, affects the generation of ventro-medial precursors and differentiated cells (Gutin et al., 2006). Moreover, Fgfr1, rather than Fgfr3, is required for generating telencephalic midline structures such as the septum, midline glial cell populations, and all three forebrain commissures (Smith et al., 2006; Tole et al., 2006).

Given the complexity of signaling and considerable overlap in their expression domains, Fgfs are likely to act in concert and potentially compensate for the loss of Fgf signaling in nearby regions. In this regard, although Fgfr3 may not play a crucial role in the development of midline structures as a sole receptor, the specific role of Fgfr3 in the correct development of other areas of the cortex has not been fully addressed. For example, as Fgfr3 is expressed in a low mediodorsal to high ventro-lateral pattern of expression, it may play a role in the formation of structures such as the rhinal and piriform cortices, hippocampus, amygdala, and striatum, where expression of this receptor is known to be high during development, perhaps leading to abnormalities in cortical connectivity. In support of this hypothesis, an increase in caudo-lateral cortical size was reported in our previous study of the gain-of-function mutations in *Fgfr3* (Thomson et al., 2009).

In the present study, we set out to determine whether Fgfr3 may play a role in controlling overall brain size and the development of the cerebral cortex by investigating the phenotype of *Fgfr3* knockout (*Fgfr3*$^{-/-}$) mice. We found that the overall size of the forebrain, including the cerebral cortex and the hippocampus, was reduced in *Fgfr3*$^{-/-}$ mice, with a particular reduction in the caudo-ventral region of the telencephalon. We then addressed whether this change may cause defects in the development of major axonal projections within the telencephalon. We have investigated the wiring between the cortical hemispheres and the thalamus by dye tracing, and between the cortex and other cerebral structures using diffusion magnetic resonance imaging (dMRI) and tractography.

TABLE 1. Brain Weight of the *Fgfr3*$^{-/-}$ Mice[a]

Genotype	n	Weight (mg) ± s.d.	% *Wild type*	*P* value[b]
E16.5				
Wild type	3	62.2 ± 2.74		
Fgfr3$^{+/-}$	7	64.3 ± 8.70	103.4	0.574 (NS)
Fgfr3$^{-/-}$	3	52.4 ± 3.51	84.2	0.0187
P0.5				
Wild type	5	100.0 ± 5.78		
Fgfr3$^{+/-}$	8	97.4 ± 5.06	97.4	0.424 (NS)
Fgfr3$^{-/-}$	3	87.5 ± 7.43	87.5	0.0377

[a]s.d., standard deviation.
[b]*P* values were obtained from unpaired, two-tailed Student's *t*-test.

RESULTS

Brain Weight and Overall Size Is Reduced in *Fgfr3* Knockout Mice

We first compared the gross morphology of the *Fgfr3*$^{-/-}$ brains at embryonic day (E) 13.5 (E13.5), E16.5, and at postnatal day (P) 0.5 (P0.5). As expected from the previous reports (Gutin et al., 2006; Kang et al., 2009; Paek et al., 2009), no significant difference was observed in the overall appearance of the *Fgfr3*$^{-/-}$ brains compared to control littermates (data not shown). The overall brain weight at E16.5 and P0.5 was then compared after careful dissection. The weight of the *Fgfr3*$^{-/-}$ brains at E16.5 was reduced by 16.7% compared to that of wild type brains ($n = 3$ for each genotype, $P = 0.0187$) (Table 1). At P0.5, the weight of the *Fgfr3*$^{-/-}$ brains was also reduced by 12.5% compared to that of wild type brains ($n = 5$ wild type, $n = 3$ *Fgfr3*$^{-/-}$, $P = 0.0377$). No statistically significant differences in the overall weight of heterozygous *Fgfr3*$^{+/-}$ brains compared to wild type brains was observed (*Fgfr3*$^{+/-}$ $n = 7$ at E16.5, $n = 8$ at P0.5).

Next, we examined the morphology of the cerebral cortex of *Fgfr3*$^{-/-}$ mice in Nissl-stained sections (Fig. 1). We compared coronal sections along the rostrocaudal axis, but no gross difference was observed in the cortical morphology of *Fgfr3*$^{-/-}$ mice compared to those of wild type or heterozygous *Fgfr3*$^{+/-}$ mice at E13.5 (data not shown). Furthermore, at E18.5, the cortical wall, the hippocampus, and the thalamus of the *Fgfr3*$^{-/-}$ mice were similar to that of wildtype mice, but had a smaller appearance ($n = 3$ wild type and $n = 5$ *Fgfr3*$^{-/-}$; Fig. 1). More detailed examination revealed that the morphology of the cerebral cortex, up to the level in which the thalamus and the habenular commissure are present (plate 8 in Jacobowitz and Abbott, 1997), was similar in *Fgfr3*$^{-/-}$ and wild type mice (Fig. 1A–D and data not shown). In accordance with previous reports (Smith et al., 2006; Tole et al., 2006), commissural structures including the corpus callosum and hippocampal commissure were present in the *Fgfr3*$^{-/-}$ cortex (Fig. 1C,D). The anterior commissure was present but appeared reduced in size (discussed later). The lateral olfactory tract appeared to be retained in the *Fgfr3*$^{-/-}$ cortex (Fig. 1A,B and C,D). In contrast, in the caudo-ventral cortex, the amygdala, including the anterior part of the basolateral amygdaloid nucleus (BLA), the anterior part of the medial amygdaloid nucleus (MeA), and the posterior medial cortical amygdaloid nucleus (PMCo), appeared to be disproportionately reduced in size in the *Fgfr3*$^{-/-}$ cortex compared to wild type brains (Fig. 1E,F).

Fgfr3 Knockout Mice Display a Reduction in the Volume of the Cortex and Hippocampus

In order to address the consequence of removing the *Fgfr3* gene in postnatal stages, we next quantified the size difference of wild type and *Fgfr3*$^{-/-}$ brains by performing volumetric analyses using MRI T2 images (Fig. 2). By comparing the MRI images to the mouse brain atlas (Paxinos, 2001), a region of interest (ROI) for the cerebral cortex was defined in each 40-μm-thick coronal image

throughout the rostro-caudal axis using MRIcro software (Chris Rorden, Georgia Institute of Technology, Atlanta, GA) (Fig. 2A). The analysis revealed that the volume of the cerebral cortex was reduced by 26.7% in the *Fgfr3*$^{-/-}$ brains compared to wild type ($n = 3$ each genotype, $P = 0.001$), while the cortical volume was similar between the *Fgfr3*$^{+/-}$ and wild type brains ($n = 3$ each genotype) (Fig. 2B). In order to investigate whether the reduced cortical volume was caused by a change along a particular axis, we compared images along the rostro-caudal (length), medial to lateral (width), and dorsal to ventral (height) axes (Fig. 2C, right panel). The rostro-caudal length of the *Fgfr3*$^{-/-}$ cortex was reduced by 10.7% compared to controls ($n = 4$ wild type and $n = 5$ *Fgfr3*$^{-/-}$, $P = 0.011$), while the width and the height at the widest and highest points of the cortex were also reduced in *Fgfr3*$^{-/-}$ by 8.7 and 9.2% ($P = 0.0017$ and 0.017), respectively (Fig. 2C left panel). This showed that the *Fgfr3*$^{-/-}$ cortex was reduced in size more or less equally in all axes.

Using MRI T2 images, volumetric analyses were also performed by defining the ROI for the hippocampus in each coronal image throughout the rostro-caudal extension (Fig. 2D). The volume of the hippocampus was reduced by 16.3% in *Fgfr3*$^{-/-}$ brains compared to that of wild type brains ($n = 4$ wild type, $n = 5$ *Fgfr3*$^{-/-}$, $P = 0.023$), while there was no statistically significant difference between the *Fgfr3*$^{+/-}$ and wild type brains ($n = 4$ wild type, $n = 6$ *Fgfr3*$^{+/-}$) (Fig. 2E).

Finally, we analyzed the volumes of the latero-ventral region of the telencephalon, which included the piriform cortex and the amygdala (Fig. 2F), where a further reduction of size was evident at E18.5 (Fig. 1) and at P7.5 (data not shown). For the piriform cortex, we divided the ROI into rostral and caudal regions, and for the amygdala ROI we included the lateral amygdaloid nucleus (LA), the basolateral amygdaloid nucleus, anterior part (BLA), the amygdaloid nucleus, anterior part (MeA), and the posterior nuclei. The analysis showed that the volume of the rostral piriform cortex was reduced by 19.8% ($n = 4$ wild

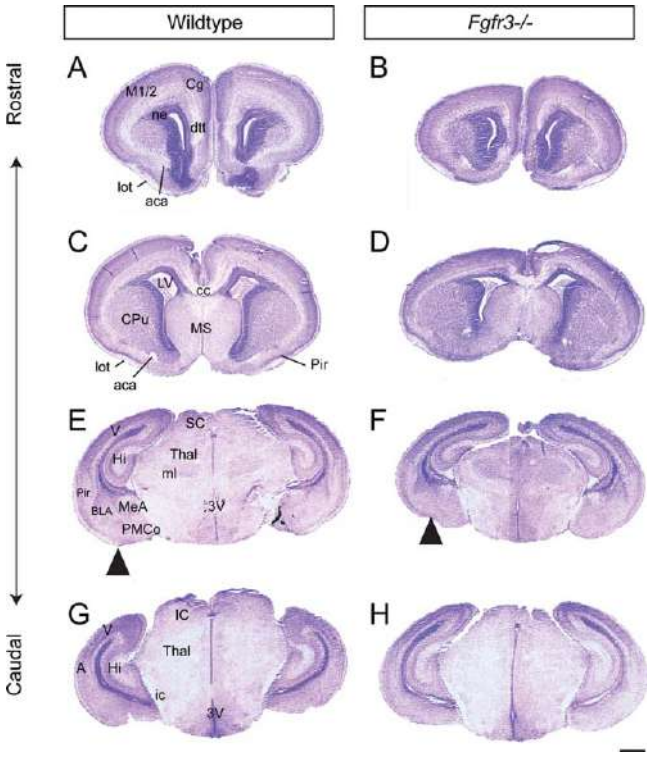


Fig. 1.

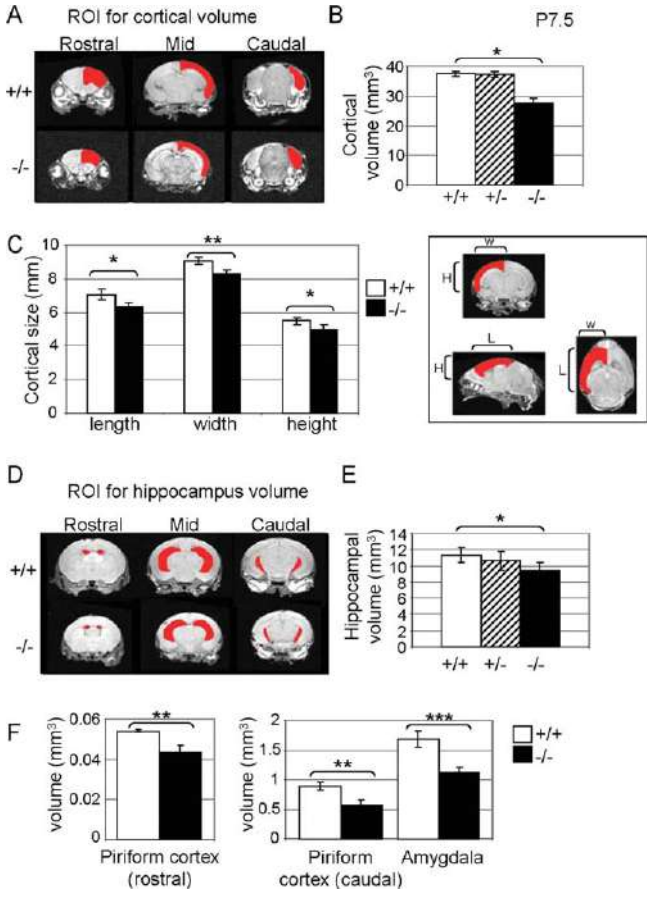


Fig. 2.

type, $n = 5$ *Fgfr3*$^{-/-}$, $P = 0.0017$). A larger decrease was observed in the volume of the caudal piriform cortex and the amygdala of 36.1% and 32.0%, respectively ($n = 4$ wild type, $n = 4$ *Fgfr3*$^{-/-}$; $P = 0.011$ and $P = 0.00047$).

In summary, the volumetric studies of the cerebral cortex and the hippocampus supported the observed reduction in overall brain size, including a marked reduction in the caudo-ventral telencephalon, including the piriform cortex and the amygdala.

Reduced Cortical Wall Thickness in *Fgfr3* Knockout Mice at P7.5

Using Nissl-stained sections, we compared the cortical thickness of distinct cortical areas in the wildtype and *Fgfr3*$^{-/-}$ brains. We first defined the prospective primary motor (pM1), somatosensory barrel subfield (pS1BF), auditory (pAu1), and visual areas (pV1) in E18.5 cortex using an embryonic mouse brain atlas (Jacobowitz and Abbott, 1997). Measurements of the cortical thickness along these areas using ImageJ software (NIH, Bethesda, MD) showed no statistically significant differences between *Fgfr3*$^{-/-}$ mice and wild type at this embryonic stage ($n = 4$ wild type, $n = 5$ *Fgfr3*$^{-/-}$) (data not shown). We next examined whether the overall thickness of these areas might have changed at later developmental stages. Using the T2-weighted MRI images, a statistically significant reduction of the cortical thickness was indeed observed in all M1, S1BF, Au1, and V1 areas studied at P7.5 ($n = 4$ wild type, $n = 5$ *Fgfr3*$^{-/-}$, $P = 0.02$–0.03) (Fig. 3). The reduction was larger in M1 and V1 (18.8 and 19.9% reduction, respectively) compared to that in the S1BF and Au1 (9.9 and 15.5% reduction).

Fgfr3 Regulates Neurogenesis in the Developing Cortex

In order to see whether the reduction of cortical volume in the *Fgfr3*$^{-/-}$ cortex is associated with a decrease in cortical progenitor cell proliferation, we performed a bromodeoxyuridine (BrdU) labelling study at E13.5. Time-mated females were injected with BrdU for 1 hr prior to sacrificing. Immunohistochemistry was performed with BrdU/Pax6 and BrdU/T-box brain gene 2 (Tbr2) on consecutive sections to identify proliferating radial glia (Pax6-positive) and intermediate neuronal progenitors (Tbr2-positive) (Englund et al., 2005). The analyses were performed at rostral and caudal levels of the dorsal cortex, selected based on the morphological equivalent of plates 1 and 9, respectively (Jacobowitz and Abbott, 1997). Cells were counted in a 50-μm channel that spanned the ventricular zone and subventricular zone of both right and left hemispheres and averaged (n = each genotype).

The results showed that there was little difference in cell proliferation between the wild type and *Fgfr3*$^{-/-}$ dorsal cortex at the rostral level, with no statistically significant difference in total BrdU-labelled cells (40.4 ± 8.7 and 44.8 ± 8.7 cells in wild type and *Fgfr3*$^{-/-}$, respectively; $P = 0.06$), Pax6- (69.7 ± 4.3 and 82.2 ± 15.3 cells in wild type and *Fgfr3*$^{-/-}$ brains, respectively; $P = 0.12$), or Tbr2-positive cells (24.5 ± 1.8 and 29.0 ± 6.6 cells in wild type and *Fgfr3*$^{-/-}$, respectively; $P = 0.16$). Similarly at the caudal level, no statistically significant differences were observed in BrdU$^+$-labelled cells (28.7 ± 1.5 and 27.3 ± 2.9 cells in wild type and *Fgfr3*$^{-/-}$, respectively; $P = 0.25$) or Pax6-positive cells (54.0 ± 2.8 and 51.5 ± 6.5 cells in wild type and *Fgfr3*$^{-/-}$ brains, respectively; $P = 0.29$).

Interestingly, however, the number of Tbr2-positive cells in *Fgfr3*$^{-/-}$ was 137.7% compared to wild type (22.7 ± 3.9 and 31.7 ± 2.5 cells in wild type and *Fgfr3*$^{-/-}$, respectively; $P = 0.014$). We, therefore, also examined the number of proliferating intermediate neural progenitors that are both Tbr2- and BrdU-positive (Tbr2$^+$BrdU$^+$) and the ratio of proliferating intermediate neural progenitors among total proliferating cells (Tbr2$^+$BrdU$^+$/BrdU$^+$). Although the changes in the number of Tbr2$^+$BrdU$^+$ cells was not statistically significant (3.3 ± 2.0 and 5.8 ± 1.0 cells in wild type and *Fgfr3*$^{-/-}$, respectively; $P = 0.065$), the ratio of Tbr2$^+$BrdU$^+$/BrdU$^+$ in *Fgfr3*$^{-/-}$ increased compared to wild type (0.11 ± 0.06 and 0.19 ± 0.02 in wild type and *Fgfr3*$^{-/-}$, respectively; $P = 0.035$). In contrast, there

Fig. 1. Comparison of *Fgfr3*$^{-/-}$ gross forebrain morphology at E18.5. The morphology was examined by Nissl staining of sections along the rostro-caudal axis of wild type control mice (**A,C,E,G**) and *Fgfr3*$^{-/-}$ mice (**B,D,F,H**). While reduced overall, the reduction in the size of the *Fgfr3*$^{-/-}$ forebrain appeared to be particularly prominent in the caudo-ventral telencephalic region (arrowheads in E,F). Scale bar = 500 μm. A, auditory cortex; aca, anterior commissures, anterior part; BLA, basolateral amygdaloid nucleus, anterior part; cc, corpus callosum; Cg, cingulum; CPu, caudate putamen (striatum); dtt, dorsal tenia tecta; Hi, hippocampus; ic, internal capsule; IC, inferior colliculus; lot, the lateral olfactory tract; LV, lateral ventricle; M1/2, primary and secondary motor cortex; MeA, amygdaloid nucleus, anterior part; ml, medial lemniscus; MS, medial septal nucleus; ne, neuroepithelium; Pir, piriform cortex; PMCo, posterior medial cortical amygdaloid nucleus; SC, superior colliculus; Thal, thalamus; 3V, 3rd ventricle; V, visual cortex.

Fig. 2. Quantitative analyses of *Fgfr3*$^{-/-}$ brains at P7.5 using MRI T2-weighted images. **A:** Using the coronal images, a region of interest (ROI) that defined the cerebral cortex was marked at each 40-μm-thick image throughout the rostro-caudal axis using MRIcro software. Representative ROIs marking the cortex in rostral, middle, and caudal levels are shown in red. **B:** The cortical volume of *Fgfr3*$^{-/-}$ mice was reduced by 26.7% compared to that of wild type, while the cortical volumes of *Fgfr3*$^{+/-}$ and wild type were similar ($n = 3$ each genotype). The asterisk indicates statistically significant differences in the volumes by two-sample t-tests comparing wild type and *Fgfr3*$^{-/-}$ ($P = 0.001$, $n = 3$ each). Analysis and the values were of one hemisphere. **C:** The three dimensions of the cerebral cortex were compared in T2-weighted structural images obtained by MRI ($n = 4$ wild type control and $n = 5$ *Fgfr3*$^{-/-}$). The width, height, and length of the cortical ROI used for cortical size measurements are indicated on the right. A consistent and statistically significant reduction in the length, width, and height was observed (left). **D:** The hippocampus ROI (regions mainly consisting of CA1, CA2, CA3, and dentate gyrus) was marked for each image slice throughout the rostro-caudal axis. Representative ROIs marking the hippocampus in rostral, mid, and caudal level are shown in red. **E:** The hippocampal volume was reduced in *Fgfr3*$^{-/-}$ mice by 16.3% compared to control ($n = 4$ wild type; $n = 6$ *Fgfr3*$^{+/-}$; $n = 5$ *Fgfr3*$^{-/-}$). The asterisk indicates a statistically significant difference of the volumes by two-sample t-test comparing wild type and *Fgfr3*$^{-/-}$ ($P = 0.023$, $n = 4$ wild type; $n = 5$ *Fgfr3*$^{-/-}$). **F:** The rostral aspect of the piriform cortex showed reduction of 19.8% ($n = 4$ wild type, $n = 5$ *Fgfr3*$^{-/-}$, $P = 0.0017$) in *Fgfr3*$^{-/-}$ mice. The volumetric analyses of the caudo-lateral region of the *Fgfr3*$^{-/-}$ cortex show a volume reduction of the caudal piriform cortex and amygdala by 36.1% ($P = 0.011$) and 32.0% ($P = 0.00047$) ($n = 4$ wild type, $n = 4$ *Fgfr3*$^{-/-}$), respectively.

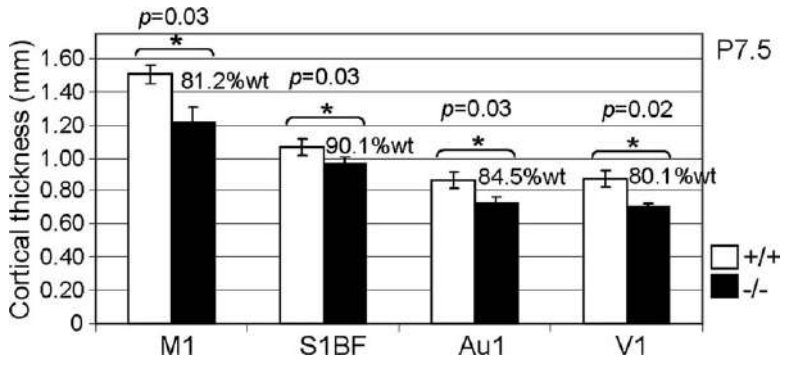


Fig. 3. Comparison of the cortical thickness in the rostro-caudal areas in *Fgfr3*$^{-/-}$ mice. **A:** The cortical thickness of primary motor (M1), somatosensory barrel subfield (S1BF), auditory (Au1), and visual areas (V1) was compared at P7.5 using the T2-weighted MRI images. A statistically significant reduction of the cortical thickness was observed in all areas ($n = 4$ wild type, $n = 5$ *Fgfr3*$^{-/-}$, P values as indicated).

was no statistically validated difference in the number of Pax6^{+}BrdU^{+} cells (24.0 ± 3.5 and 22.3 ± 3.7 cells in wild type and *Fgfr3*$^{-/-}$, respectively; $P = 0.30$) or Pax6^{+}BrdU^{+}/BrdU^{+} (0.9 ± 0.03 and 0.91 ± 0.01 cells in wild type and *Fgfr3*$^{-/-}$, respectively; $P = 0.41$). This result may imply that proliferating cells are delayed in leaving the SVZ in caudal regions of the *Fgfr3*$^{-/-}$ cortex, or that the Pax6-Tbr2-Tbr1 sequential gene expression (Englund et al., 2005) is delayed in radial glia at the Tbr2-expressing stage. Altogether these results indicate that Fgfr3 plays a subtle role early in neurogenesis (E13.5) by regulating the exit of intermediate neural progenitors from the subventricular zone.

Dysmorphology of the Caudo-Ventral Telencephalon in *Fgfr3* Knockout Mice

Given the notable decrease in the size of the caudo-ventral telencephalon, we sought to better understand the cellular morphology of this region. To do this, we investigated cell type and cell density in the amygdala, which included the nuclei of the basolateral amygdala, the central amygdala, and the basomedial amygdala, and in the posterior piriform cortex (layers I–III) at E18.5 (Fig. 4A). There was no change in the cellular density of the amygdala in *Fgfr3*$^{-/-}$ mice (Fig. 4B), suggesting that the decrease in volume of this region is due to decreased cell number, not due to decreased interstitial space or decreased intracellular space. In contrast, the piriform cortex of *Fgfr3*$^{-/-}$ mice showed an increased cellular density of approximately 24% compared to wild type (Fig. 4B′), suggesting that there was a decrease in interstitial space or decreased intracellular space. Since the piriform cortex is composed of multiple layers, each with differing cellular densities, further analysis was performed to determine which of the layers was affected. Since layers Ia, Ib, and II have distinct boundaries, the width of these layers was measured (Fig. 4C,C′). Layers Ib and II of *Fgfr3*$^{-/-}$ mice were significantly thinner than wild type by 35 and 42%, respectively (Fig. 4D). Overall, there was an average decrease of the layers I–II in *Fgfr3*$^{-/-}$ mice by 90 μm, or 40% of wild type. There was an inverse correlation between the layer thickness and cell density such that in layers Ib and II of *Fgfr3*$^{-/-}$ mice, there was an increase in cell density compared to wild type of 50 and 25%, respectively (Fig. 4E).

Counts of BrdU-labelled cells (Fig. 4F,F′) revealed that there was a greater proportion of cells undergoing proliferation at E18.5 in layer Ib, but not in the other layers (Fig. 4G). By contrast, a small but significant decrease in the proportion of BrdU-labelled cells in the amygdala was found in *Fgfr3*$^{-/-}$ mice compared to wild type mice (Fig. 4I). Tbr1 is a marker of developing and mature telencephalic excitatory neurons (Hevner et al., 2001). The number of Tbr1-positive neurons in the piriform cortex and the amygdala was counted (Fig. 4J–M). A slight, but not statistically significant, decrease in the proportion of Tbr1-positive neurons was observed in the piriform cortex and amygdala. Nevertheless, the distribution of Tbr1-positive neurons was concordant with the change in cell density within the piriform layers. The glutamate decarboxylase 67-kDa isoform (GAD67 or Gad1) catalyses the production of GABA and can serve as a marker of GABAergic inhibitory neurons, which are a prominent cell population of the amygdala. While a decrease in the number of GAD67-positive cells was observed in the amygdala (Fig. 4P,Q), an 8-fold increase in the proportion of GAD67-positive cells was found in layer Ia of the piriform cortex in *Fgfr3*$^{-/-}$ mice compared to wild type (Fig. 4N,O).

We further sought to identify the cell types that had undergone proliferation around birth that were quantified in the above experiment. To do this, immunohistochemistry was performed for BrdU and either GFAP, the oligodendrocyte precursor marker Olig2, or the neuronal marker NeuN (Rbfox3). Representative double-immunofluorescence images of the piriform cortex and amygdala are shown in Figure 5. In the piriform cortex, approximately 60% of BrdU-positive cells were GFAP-positive, 30% were NeuN-positive, and the remaining cells were neither GFAP-, Olig2-, nor NeuN-positive. In the amygdala, however, 90% of BrdU-positive cells were also GFAP-positive cells. The majority of the remaining BrdU-cells were neither GFAP- nor NeuN-positive. On very few occasions, BrdU-positive cells were also Olig2-positive (data not shown). The difference between GFAP-positive and NeuN-positive immunoreactivity of BrdU-positive cells between *Fgfr3*$^{-/-}$ and wild type mice were quantified (Table 2). Only a significant decrease in GFAP-positive cells was observed in the amygdala in *Fgfr3*$^{-/-}$ mice.

In summary, a slight decrease in cell proliferation as well as the number of GABAergic inhibitory neurons was observed in the amygdala of *Fgfr3*$^{-/-}$ mice. In the piriform cortex of *Fgfr3*$^{-/-}$ mice, there was an increase in cell density, but a reduction in the thickness of each of the

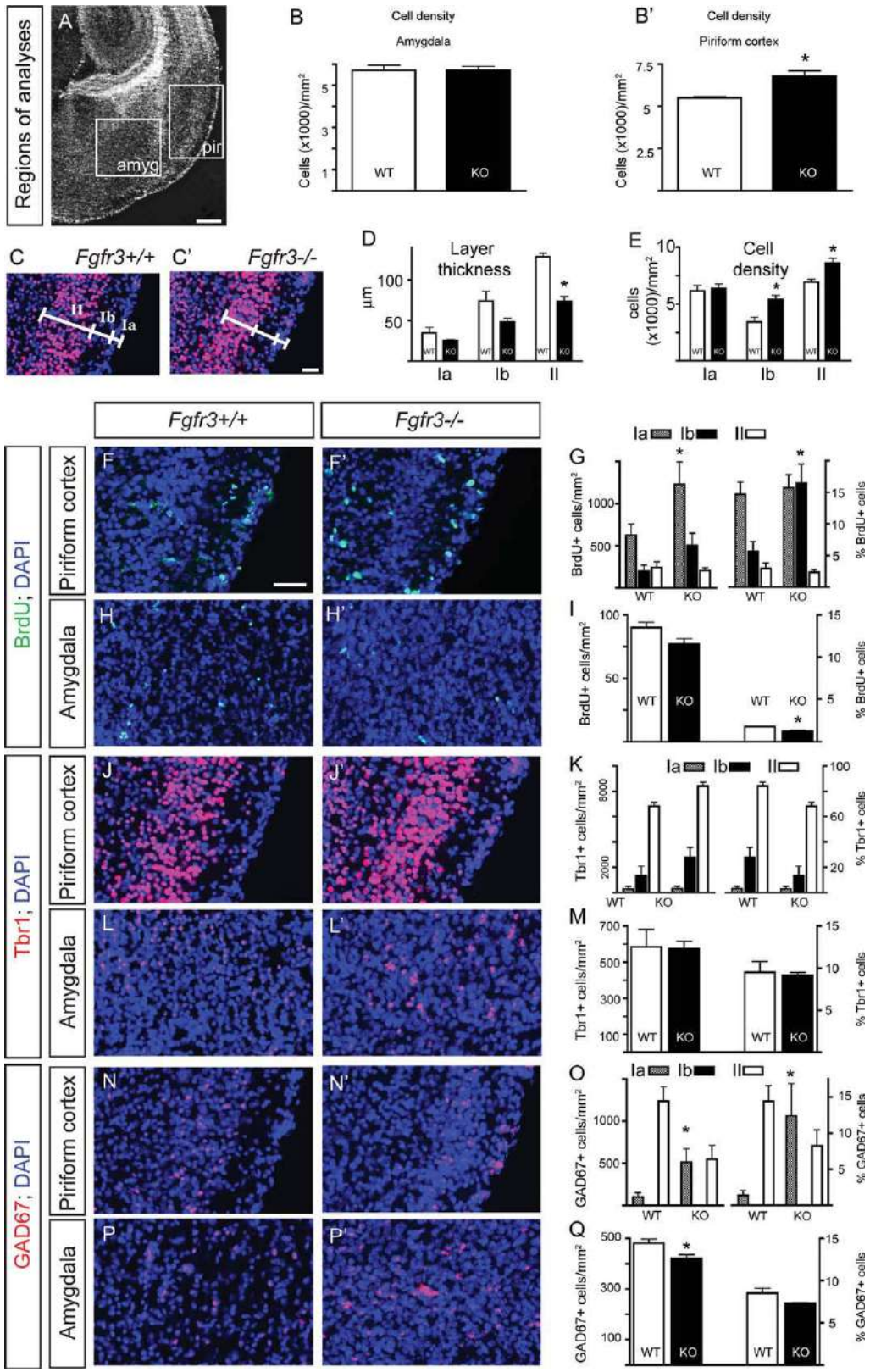


Fig. 4. Hypoplasia of the amygdala and piriform cortex is associated with dysplasia of GABAergic neurons at E18.5. **A:** Cell number and morphology were investigated in two caudo-ventral regions of the telencephalon: the amygdala (including the basolateral amygdala, the central amygdala, and the basomedial amygdala) and the posterior piriform cortex (layers I–III). Cell densities in the amygdala were unchanged, but significantly higher in the piriform cortex (**B, B′**). A breakdown of the lateral piriform cortex layers (**C, C′**) revealed a decreased layer thickness (**D**), but also a concordant increase in cell density (**E**). To examine the nature of this dysmorphology, counts were made of the number of newborn cells marked via BrdU injection at E18.5, the number of projection neurons marked by anti-Tbr1, and the number of GABAergic neurons marked by anti-GAD67. There was a significant increase in the number of BrdU cells in layer Ia, but only a significant increase in the proportion of BrdU$^+$ cells in layer Ib (**F,F′,G**). A decrease in BrdU$^+$ cells was observed in the amygdala (**H,H′,I**). There was a trend for a decrease in the number and proportion of Tbr1$^+$ cells in the piriform cortex and amygdala, although neither region was statistically significant between genotypes (**J–M**). A significant decrease in GAD67$^+$ cells was observed in layer II, but an increase was seen in layer Ia (**N,N′,O**). A decrease in GAD67$^+$ cells was found in the amygdala (**P,P′,Q**). *$P < 0.05$ compared to wild type, *t*-test, or two-way ANOVA with post-hoc *t*-test. Scale bars = 200 μm (A); 50 μm (C,C′; F–P).

TABLE 2. Cell Type Profiles at E18.5 Following 1-Hr BrdU Labeling in the Ventrocaudal Telencephalon[a]

	Amygdala		Piriform cortex	
Immunoreactivity	*Fgfr3*$^{+/+}$	*Fgfr3*$^{-/-}$	*Fgfr3*$^{+/+}$	*Fgfr3*$^{-/-}$
Anti-GFAP	86 ± 2	75 ± 3*	59 ± 2	65 ± 3
Anti-NeuN	nd	nd	24 ± 9	30 ± 7

[a]Cells counts are expressed as a percentage of BrdU$^+$ cells ± s.e.m. nd, not detected.
*$P < 0.05$ compared to *Fgfr3*$^{+/+}$; unpaired, two-tailed Student's *t*-test (n = 3 mice).

layers, resulting in a smaller piriform cortex. Moreover, in the piriform cortex of *Fgfr3*$^{-/-}$ mice, we observed an increase in late embryonic cellular proliferation as well as in the number of GABAergic inhibitory neurons. The decrease in proliferation around the time of birth is likely to impact on the number of glial-lineage cells.

Fgfr3 Knockout Mice Display Defects in Early Thalamocortical Axon Guidance

As we have described above, there is a significant reduction of the cortical size in *Fgfr3*$^{-/-}$ mice. Thus, we next examined whether this defect might lead to abnormalities in the targeting and/or overall topography of projections into the cortex. Thalamocortical axons navigate through the ventral telencephalon at early embryonic stages to topographically target neocortical areas at E18.5 (Lopez-Bendito and Molnar, 2003). Thus, we first determined whether *Fgfr3* might influence the early guidance and topography of thalamocortical connectivity during development. At E14.5, we observed some indications that thalamocortical axon guidance had been disrupted in the *Fgfr3*$^{-/-}$ brains compared to wild type (Fig. 6). Although dye-tracing studies vary in the number of axons labeled, we consistently found less thalamocortical axons projecting through the ventral telencephalon and arriving at the striatocortical boundary in the *Fgfr3*$^{-/-}$ brains (Fig. 6). Some of these axons were defasciculated at the level of the ventral telencephalon. The internal capsule was also disrupted and this effect was stronger in the caudal levels (Fig. 6 and data not shown). In contrast, corticofugal axons appeared to be relatively normal at this stage (data not shown).

We performed double dye-tracing studies from parietal (DiA) and occipital (DiI) cortical areas at E18.5 when interconnectivity from cortex and thalamus has been established. Although early guidance defects were observed for thalamocortical axons, no appreciable abnormalities were observed in the topography of thalamocortical connectivity (Fig. 7A–D). Altogether, these results indicate that the removal of the *Fgfr3* gene in both the cortex and the thalamus does not cause any major failure or abnormalities in the topographic sorting of thalamocortical axons and corticofugal axons.

dMRI and Tractography Reveals Caudal Cortical Tract Deficits in *Fgfr3* Knockout Mice

The results showed that extrinsic cortical projections, such as thalamocortical axons, are not severely affected by the reduction of cortical size observed in *Fgfr3*$^{-/-}$ mice. However, given the high expression of *Fgfr3* in the embryos in the caudal aspects of the cortex, we aimed to determine whether intrinsic cortical axonal tracts might be affected. To achieve a three-dimensional appreciation of cortical tracts and their size, we performed dMRI on the brains of P0 mice and used tractography to plot the streamlines from ROIs. Tractography demonstrated that basocaudal telencephalic tracts, exemplified by tracts comprising the anterior commissure, were in fact reduced in *Fgfr3*$^{-/-}$ mice (Fig. 8). The anterior commissure consists of anterior and posterior arms (Sturrock, 1978). In addition to plotting the anterior arm, tractography of the anterior commissure permitted dissection of the posterior arm into lateral and caudal streamline populations. Using this approach, a reduction in the lateral and caudal streamlines, but not the rostral streamlines, was found to be statistically different between *Fgfr3*$^{-/-}$ and wild type mice (Fig. 8C). This difference was observed despite there being no difference in the volume of the anterior commissure ROI. No streamline number differences were seen between *Fgfr3*$^{+/-}$ and wild type mice (data not shown). The specificity of the caudal tract deficit was investigated using an ROI placed in a region that spanned the fimbria, the stria terminalis, the dorsal internal capsule connecting the cortex and thalamus, and the ventral internal capsule (Fig. 8D). Of these ROIs, only that of the stria

Fig. 5. Representative immunohistochemistry of BrdU-labeled cells in the piriform cortex and amygdala of E18.5 wild type mouse brains. Cells were marked via 1-hr BrdU injection. **A,B:** The majority of BrdU$^+$ cells were also immunopositive for GFAP (open arrowhead). Arrow shows cells BrdU$^-$ and GFAP$^+$. Cells BrdU$^+$ and GFAP$^-$ are indicated by the closed arrowhead. **C:** Approximately 30% of BrdU$^+$ cells were also immunopositive for NeuN in the piriform cortex (open arrowhead). Arrow points to cells BrdU$^-$ and NeuN$^+$. **D:** No BrdU$^+$ cells were immunopositive for NeuN in the amygdala. Closed arrowhead indicates cells BrdU$^+$ and NeuN$^-$. Scale bar = 20 μm.

Fig. 6. Early thalamocortical guidance defects in *Fgfr3* knockout mice. DiI crystals were placed in the dorsal thalamus (dTh) of *Fgfr3*$^{-/-}$ ($n = 2$) and wild type ($n = 2$) mice at E14.5. **A–D:** Coronal sections showing TCAs labeled with DiI in wild type brains. The normal route of TCAs along the ventral telencephalon is indicated by open arrowheads in D. **E:** Schema representing the TCAs pathfinding at the ventral telencephalon in wild-type brains. **F–I:** Injection of DiI in the dTh of the *Fgfr3*$^{-/-}$ brains showed early guidance defects of TCAs at the ventral telencephalon. Axons appear stalled at the level of the internal capsule and some axons are defasciculated from the main bundle (open arrowhead in I). The structure of the internal capsule is disrupted in the *Fgfr3*$^{-/-}$ brains (solid arrowheads in G). Less TCAs seem to navigate toward the neocortex (NCx) in the *Fgfr3*$^{-/-}$ brains compared to the wild type. **J:** Schema representing the TCAs pathfinding at the ventral telencephalon in the *Fgfr3*$^{-/-}$ brains. Scale bars in A and F indicate 500 μm; B–D and G–I, 500 μm. Hyp, hypothalamus.

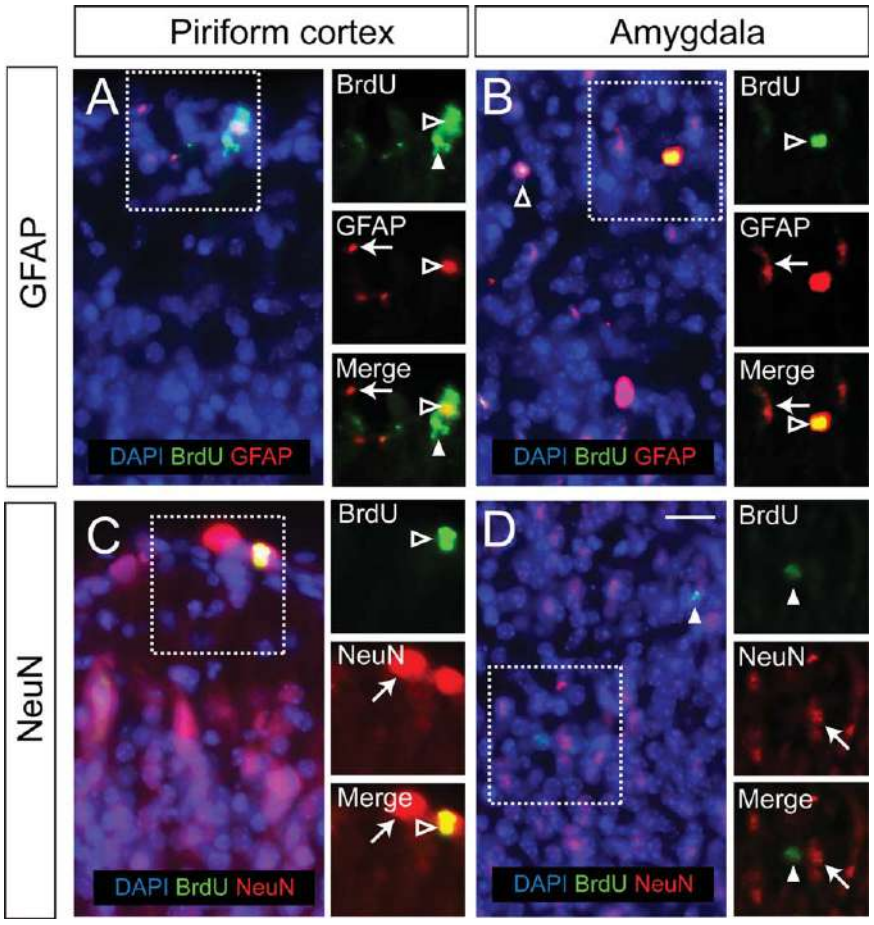


Fig. 5.

terminalis consists of axon tracts that project from the bed nucleus within the amygdala (Dong et al., 2001). A significant reduction of streamlines seeded at the stria terminalis was observed, but not in the other streamline populations (Fig. 8F). Furthermore, no streamline differences were noted between genotypes when ROIs were placed in the splenium of the corpus callosum or in the hippocampal commissure at the midline (data not shown) indicating no major deficits in these structures.

DISCUSSION

This study showed that the brains of *Fgfr3*$^{-/-}$ mice are significantly smaller compared to littermate controls as early as E16.5 (Table 1). Analysis of the Nissl-stained paraffin sections as well as the T2-weighted MRI images revealed that while the general structure of the forebrain was normal, the overall size of the forebrain appeared smaller, with a particular reduction in the caudo-ventral region of the telencephalon (Fig. 1). The volumetric analyses of the cerebral cortex and the hippocampus supported the reduction in the overall brain size, as well as a specific reduction of the caudo-ventral cortical regions including the piriform cortex and the amygdala in the *Fgfr3*$^{-/-}$ mice

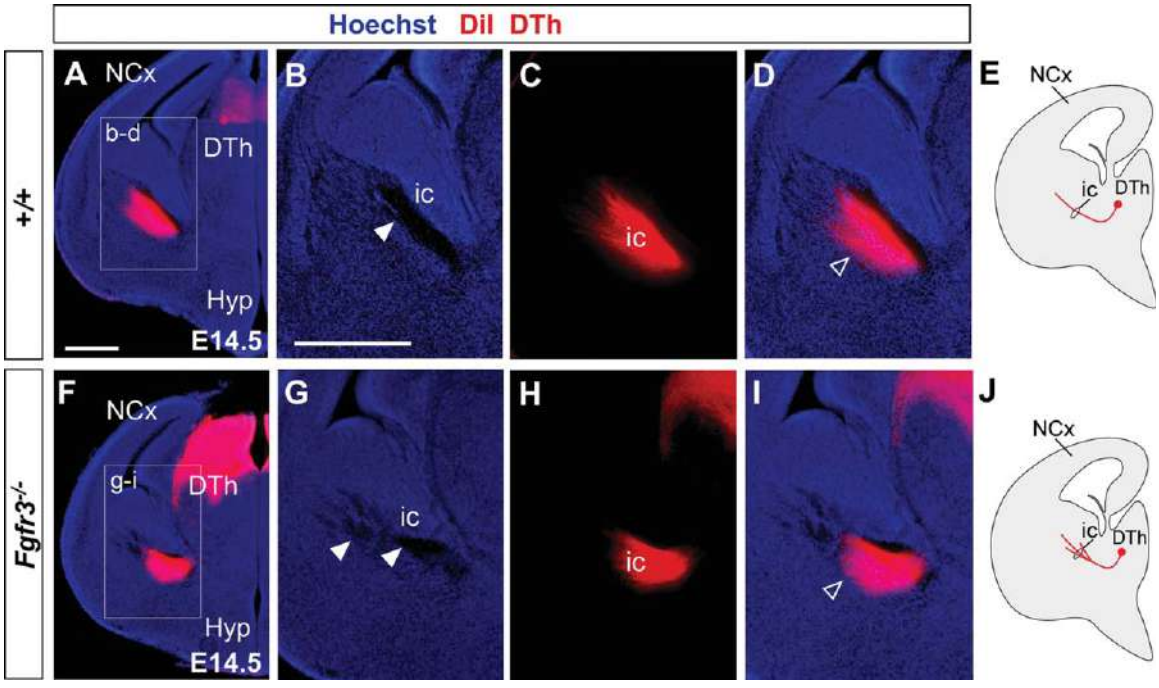


Fig. 6.

at P7.5 (Fig. 2). The cortical thickness was reduced in all M1, S1BF, Au1, and V1 cortical areas in *Fgfr3*$^{-/-}$ mice at postnatal ages, while not at E18.5 (Fig. 3). There was no statistically significant change in proliferation of dorsal cortical progenitors in the *Fgfr3*$^{-/-}$ cortex. However, a decrease in cell proliferation, as well as that of the number of GABAergic interneurons, was observed in the amygdala of *Fgfr3*$^{-/-}$ mice at E18.5 (Fig. 4, Table 2). In contrast, in the piriform cortex, a smaller size was mostly caused by a reduction in the layer thickness accompanying an increase in cell density, as well as that of the number of GABAergic neurons. In terms of wiring, some defasciculation defects were observed in *Fgfr3*$^{-/-}$ mice in the ventral telencephalon at E14.5, which did not lead to any major failure or abnormalities in thalamocortical axon projections at later ages (Figs. 6,7). Interestingly, however, diffusion MRI and tractography revealed reduced caudolateral cerebral tracts, particularly those of the stria terminalis and anterior commissure (Fig. 8). In conclusion, these results are the first demonstration of the brain phenotype of *Fgfr3*$^{-/-}$ mice indicating a subtle role of Fgfr3 in the control of the brain size and wiring of some CNS projections.

Function of *Fgfr3* in the Control of Brain Size

This study demonstrates for the first time that the lack of Fgfr3 function leads to a reduction in brain size in vivo. This reduction is evident in terms of the overall weight and volumes of the cerebral cortex and the hippocampus (Table 1 and Fig. 2). A reduced brain size has never been reported in *Fgfr3* single knockout mice. However, care must be taken when interpreting these results with regards to the function of Fgfr3, since other Fgfrs, namely Fgfr1 and Fgfr2, are known to be expressed in overlapping regions of the brain and their contribution must be taken into account (Iwata and Hevner, 2009). Whether or not other Fgfrs may also play a role in the same region can be addressed by the examination of double and triple knockout mice, and such studies have already been reported (Gutin et al., 2006; Tole et al., 2006; Kang et al., 2009; Paek et al., 2009). A reduction in cortical size has been reported in *hGFAP-Cre;Fgfr1*$^{flox/flox}$ (Ohkubo et al., 2004) and in *Nestin-Cre;Fgfr2*$^{flox/flox}$ and *hGFAP-Cre;Fgfr2*$^{flox/flox}$ mice (Smith et al., 2006; Vaccarino et al., 2008). In particular, mice in which *Fgfr1* is deleted using a hGFAP-Cre that drives recombination in radial glia from E13.5 (*hGFAP-Cre;Fgfr1*$^{flox/flox}$) showed a 15.5% reduction in cortical size at P7.5 and 12.4% in adults (Ohkubo et al., 2004). Therefore, the level of reduction observed in the *Fgfr3*$^{-/-}$ cortex is similar to that in *hGFAP-Cre;Fgfr1*$^{flox/flox}$ mice (Fig. 2). A reduction in hippocampal size was also reported in *hGFAP-Cre;Fgfr1*$^{flox/flox}$ mice (Ohkubo et al., 2004). Our study indicates for the first time that, similar to Fgfr1 and Fgfr2, Fgfr3 is also likely to play a role in regulating cortical and hippocampal size at late embryonic and early postnatal stages.

The radial unit hypothesis (Rakic et al., 2009) proposes that cortical size is regulated by the expansion of cortical progenitors in the cortical ventricular zone early in embryogenesis, where most of the cell divisions are symmetric, producing more cortical progenitors. In contrast, the thickness of the cortical wall is regulated by divisions of intermediate neuronal progenitors in the sub-ventricular zone, which contributes to expand the postmitotic neuronal pool (Pontious et al., 2008; Rakic et al., 2009). The reduced cortical size observed in this study in the *Fgfr3*$^{-/-}$ cortex is likely to be due to a reduction in the number or rate of cell divisions that occurred early in embryonic stages. However, changes in cell proliferation were not detected by 1-hr-pulse BrdU in the *Fgfr3*$^{-/-}$ cortex at E13.5. We have previously shown that in *EIIa-Cre;Fgfr3*$^{+/K644E}$ mice, the proliferation of dorsal cortical progenitors was increased along the rostro-caudal axis according to expression levels of Fgfr3 at E11–E13 (Thomson et al., 2007, 2009). In our previous study of *EIIa-Cre;Fgfr3*$^{+/K644E}$ mice, we also investigated cell cycle parameters in cortical progenitors, leading to a discovery that the length of the cell cycle was shortened in the G1 phase, while cell cycle exit was not significantly altered in the VZ (Thomson et al., 2009). Whether similar cell cycle parameters, and other factors, such as apoptosis of the cortical progenitors are affected in the *Fgfr3*$^{-/-}$ cortex remains to be determined.

This study showed that a reduction in cortical thickness became apparent at P7.5, but not at E18.5 (Fig. 3 and data not shown). This suggests that Fgfr3 potentially regulates late neurogenesis in the sub-ventricular zone or cell survival. Analysis of the proliferating populations of Pax6- and Tbr2-positive progenitors indicated that the proliferating Tbr2-positive intermediate neural progenitors are increased in the dorsal *Fgfr3*$^{-/-}$ cortex at the caudal level without a major change in the population of Pax6-positive radial glia. This may mean that that the proliferating intermediate neural progenitors are delayed in leaving the sub-ventricular zone. Based on the observation of Pax6-Tbr2-Tbr1 sequential gene expression by Englund et al. (2005), the consequences of a radial migration delay from the sub-ventricular zone might involve a decrease or delay in the number of Tbr-1 neurons populating the upper neocortical layers or subcortical regions. In support of this, we found a small, although not statistically significant, decrease in the number of Tbr1-positive neurons in the piriform cortex (Fig. 4).

Dysmorphology of the Caudo-Ventral Telencephalon in *Fgfr3* Knockout Mice

A small and restricted region in the caudo-ventral region of the *Fgfr3*$^{-/-}$ telencephalon including the amygdala and the piriform cortex was reduced in size (Figs. 1,2,4). Fgf ligands that contribute to the formation of the caudo-ventral region of the cortex are unknown. During development, several Fgfs, including Fgf3, Fgf7, and Fgf15, are known to be expressed in the anti-hem, the putative caudo-lateral signaling center (Iwata and Hevner, 2009). The National Center for Biotechnology Information (NCBI) Gene Expression Nervous Stystem Atlas (GENSAT) database (http://www.ncbi.nlm.nih.gov/gensat) shows the expression of all Fgfr isoforms, as well as Fgf8, Fgf13, and Fgf15 in the

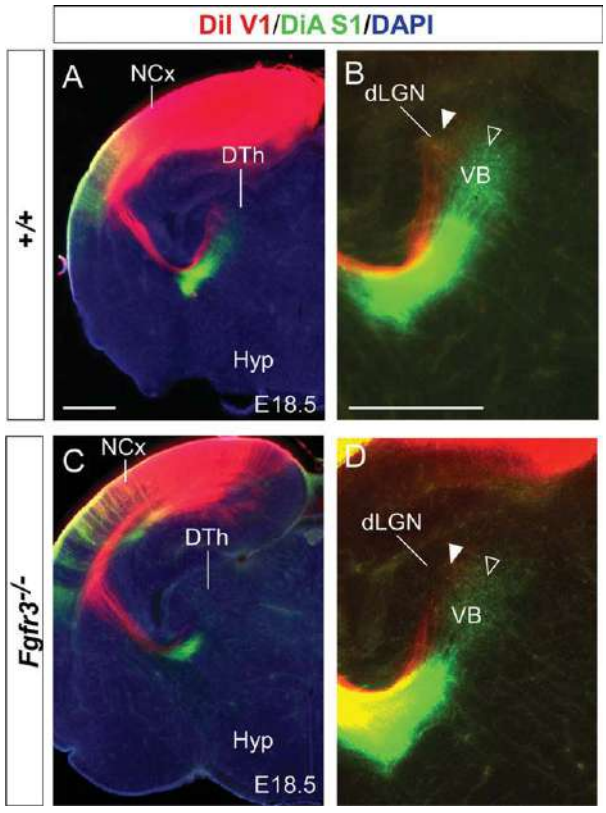


Fig. 7.

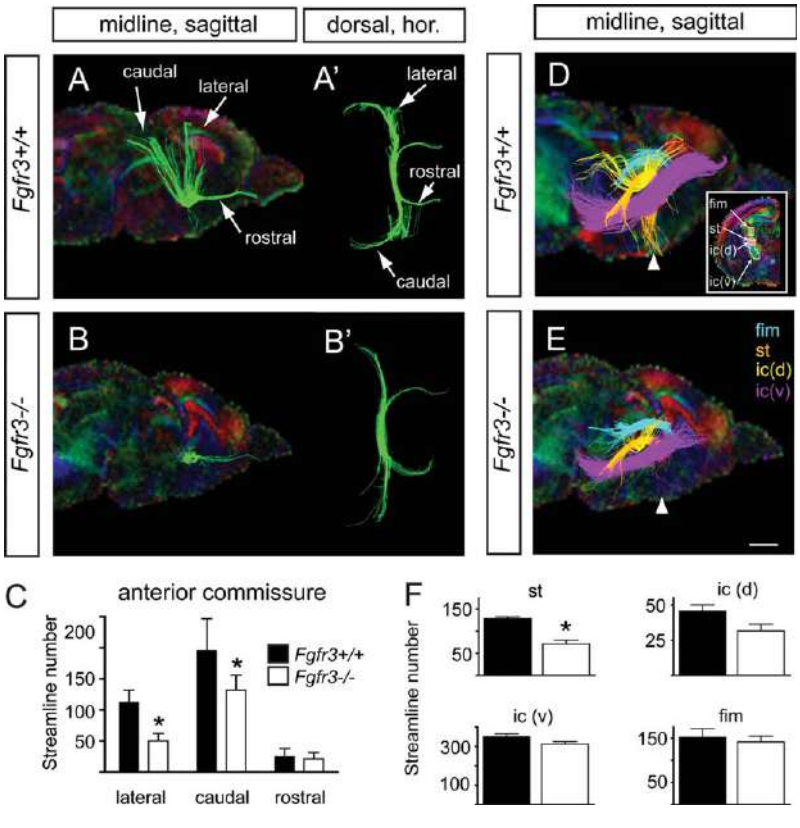


Fig. 8.

caudo-ventral region of the cerebral cortex at E15.5 and P7.

Some progenitors from the ventral pallidum, lateral pallidum, or the ganglionic eminence migrate into the basal telencephalic limbic system via the lateral cortical stream where they become excitatory projection neurons of the amygdala expressing Tbr1 (Carney et al., 2006; Hirata et al., 2009). Since there is only a small difference in the number of Tbr1-positive neurons in the amygdala of *Fgfr3*$^{-/-}$ mice (Fig. 4), defects in the differentiation and migration of these neurons is unlikely to have occurred.

Fig. 7. Overall thalamocortical topography is not affected in *Fgfr3* knockout mice. **A–D:** Coronal sections through wild type ($n = 5$; A,B) and *Fgfr3*$^{-/-}$ ($n = 4$; C,D) E18.5 brains. DiI and DiA crystals were placed in the primary visual cortex (V1) and somatosensory cortex (S1), respectively. In both wild type and *Fgfr3*$^{-/-}$ mice, DiI placement in V1 resulted in backlabeling of dLGN cells at the dorsal thalamus (filled arrowheads in B and D), and DiA placement in S1 resulted in backlabeling of VB cells at the dorsal thalamus (DTh) (open arrowheads in B and D). This topographical arrangement of connections was not altered in *Fgfr3*$^{-/-}$ brains (D). Scale bars = 500 μm in A and C, 500 μm in B and D. NCx, neocortex; Hyp, hypothalamus; dLGN, dorsal lateral geniculate nucleus; VB, ventrobasal nucleus.

Fig. 8. Tractography shows that basocaudal telencephalic tracts are reduced in *Fgfr3*$^{-/-}$ mice at P0. A–C: A reduction in the lateral and caudal streamlines generated from a ROI placed at the midline of the anterior commissure. In A, arrows point to the lateral, caudal, and rostral components of the anterior commissure streamlines set against a color map of the mouse brain in the sagittal plane. **A′:** These components in the horizontal plane, seen from the dorsal view (i.e., dorsal, hor). **B, B′:** A reduction in the lateral and caudal components of the anterior commissure streamlines can be seen. Color map bidirectional orientation key: red, mediolateral; blue, dorsoventral; green, rostrocaudal. **C:** Quantification of the number of streamlines comprising the lateral, caudal, and rostral components of the anterior commissure. $^{*}P < 0.05$, *t*-test compared to *Fgfr3*$^{+/+}$; $n = 3$. **D–F:** The specificity of the caudal tract deficit was investigated using ROIs placed at a site containing the stria terminalis (st), internal capsule dorsal (ic(d)), and ventral (ic(v)) and fimbria (fim) (inser in D). A reduction of the stria terminalis was observed, as seen in the representative image in E (compare arrowheads in D and E). Quantification of the streamline number for each tract is presented in F. $^{*}P < 0.05$, *t*-test compared to *Fgfr3*$^{+/+}$; $n = 3$. Scale bar = 1 mm for A, A′, B, B′, D, and E.

However, establishing the proportion of Tbr1-positive neurons per amygdaloid nuclei was beyond the depth of this study, and for this reason we cannot exclude the possibility that there may exist nuclei-dependent differences in glutamatergic excitatory neurons in the *Fgfr3*$^{-/-}$ basal telencephalic limbic system.

A small decrease in proliferation as well as the number of GABAergic inhibitory neurons was observed in the amygdala (Fig. 4). A decrease in GABAergic neurons was also seen in the more medial layer of the piriform cortex that was examined. However, an increase in GABAergic neurons was observed in the outer-most layer. This difference between the outer and inner piriform layers suggests a defect in GABAergic layer specification. While the glutamatergic projection neurons were not similarly affected, the layer thickness and cell density differences indicate that there is a greater dysmorphology defect occurring than that restricted to GABAergic neurons. At E18.5, those cells that are proliferating are predominantly of the glial lineage (Fig. 5, Table 2), which were reduced in the *Fgfr3*$^{-/-}$ mouse, suggesting that glia and cells derived from glial progenitors are vulnerable to deficits in proliferation at this stage of development. Finally, the changes in the amygdala, and especially the decrease in size of the piriform cortex, indicate that at a late embryonic stage, subtle morphological changes occur that presumably impact on the volume of these regions at later ages, such as at P7.5 when measured by MRI (Fig. 2).

Fgfr3 Function in Anterior Commissure Formation and Thalamocortical Axon Guidance

By diffusion magnetic resonance imaging and tractography, we have shown that there was a decrease in tracts crossing the midline via the anterior commissure (Fig. 8). One of the limitations of the dMRI and tractography used here is that streamline number changes may be due to changes in either white matter tracts or the regions they connect to. For example, decreases in stria terminalis streamline number may be due to a reduction in the volume of the septal nuclei and/or the amygdala nuclei, or alternatively, due to decreased axon growth between these regions. The decrease in the size of the basolateral and caudal telencephalon supports the former hypothesis. Other less likely but possible causes for the streamline number changes could be due to defasciculation of the axons or an increase in crossing axons, which would reduce the fractional anisotropy value and, hence, result in premature termination of the streamlines. Myelination is unlikely to influence streamline number changes because of the relatively young age of the mice investigated. Hence, the reduction in streamline number seen in the anterior commissure may not be caused by a reduction in the thickness of the anterior commissure at the midline, but rather by a reduction in those cerebral regions whose axons traverse the anterior commissure at the midline. It is likely that this decrease in the posterior arm of the anterior commissure is caused by the reduced neurogenesis caused by lack of Fgfr3 in that region during early neurogenesis.

Indeed, this study presented evidence for a role for the Fgfr3 in brain wiring. Our results indicated a subtle and transient difference in early thalamocortical axon guidance between the wild type and *Fgfr3*$^{-/-}$ brains at E14.5 (Fig. 6), which appeared to be compensated for at a later stage as the general topography of the connection was normal at E18.5 shown by double tracing studies at E18.5 (Fig. 7). Altogether, this indicates that a high expression of Fgfr3 in the early embryonic period in the caudal cortex could lead to defects in the caudal cortex including formation of the posterior arm of the anterior commissure (Fig. 8) and the possible defasciculation of axons in the internal capsule at early stages of development.

Is the Effect of *Fgfr3* Deletion in the Brain Secondary to Its Potential Role in Controlling the Size of the Embryo?

The volumes of the cerebral cortex, hippocampus, rostral and caudal piriform cortex, and amygdala, showed a varying degree of size reduction, 26.7, 16.3, 19.8, 36.1, and 32.0%, which has indicated a further reduction specifically in the caudo-ventral region of the cortex (Fig. 2F). In addition, we have measured streamlines in the corpus callosum and hippocampal commissure, which did not show any difference between the wild type and *Fgfr3*$^{-/-}$ brains (data not shown). These examples of normal brain development indicate that it is unlikely that the reduction in the size of some brain regions is caused secondarily to the overall growth of the embryo. It is reported that histological abnormalities in the skeleton can be seen in *Fgfr3*$^{-/-}$ mice as early as E18.5 (Colvin et al., 1996; Deng et al., 1996). Due to this effect in the skeleton, it would not be possible to precisely compare the size of embryos/mice. Therefore, although it is unlikely that the Fgfr3 is involved in regulating overall body size, the production of conditional knockout mice would ultimately be required to address this question.

EXPERIMENTAL PROCEDURES

Mice

All procedures were performed in accordance with the Project License under the Home Office Animal (Scientific Procedures) Act 1986, UK. The Fgfr3 knockout line (Colvin et al., 1996) was maintained by crossing the heterozygous mice with the *Fgfr3* null mutation (*Fgfr3*$^{+/-}$) to produce homozygous knockout (*Fgfr3*$^{-/-}$). Mice were maintained on the mixed background of C57BL/6 and CD1 with 2nd generation of CD1. The day of the vaginal plug was counted as E0.5.

Magnetic Resonance Imaging and Tractography

T2-weighted MRI.

After transcardiac perfusion, mouse heads were removed and fixed in 4% paraformaldehyde at 4°C with constant agitation overnight. The heads were then washed and stored in 0.01% sodium azide in phosphate-buffered saline (PBS) for a minimum of 7 days at 4°C with constant agitation.

Subsequently, the heads were incubated in sterile PBS containing 0.5% MultiHance (Bracco Diagnostics, Inc., Princeton, NJ) in 0.01% sodium azide for precisely 13 days at 4°C. On the day of MR scanning, heads were brought to room temperature and transferred to a plastic container filled with Fomblin, which was degassed under vacuum to minimise bubbles forming during MRI scanning (Tyszka et al., 2006). T2-weighted MRI scans were performed on a 7T Bruker Biospec 70/30 system at the Glasgow Experimental MRI Centre (GEMRIC). The system is equipped with a microimaging gradient insert (model BG-6) and 100-A gradient amplifiers that provide strong linear magnetic field gradient pulses of up to 1,000 mT/m. The Fomblin-filled containers were placed in a 35-mm Bruker birdcage RF resonator. A three-dimensional spin-echo sequence was acquired using the following parameters: repetition time = 600 ms; echo time = 45 ms; Field of view 19 × 11 × 12 mm; imaging matrix 238 × 137 × 150; imaging resolution 0.08 × 0.08 × 0.08 mm and four signal averages. Total scan time was 13 hr and 42 min. For the analysis of the T2-weighted MR images, we first performed the fine adjustment of the image orientation by Image J software (NIH, Bethesda, MD). Images were then viewed by MRIcro in orientations including coronal, saggital, and horizontal (Chris Rorden, Georgia Institute of Technology, Atlanta GA).

The volumes were analyzed by MRIcro placing the region of interest (ROI) in each 40-μm-thick images through rostral to caudal ranges of coronal images. Analyses were performed on one hemisphere. ROI for the cerebral cortex includes: frontal, orbital, prelimbic, motor, cingulate, insular, somatosensory, infralimbic, retrosplenial granular, ectorhinal, retrosplenial agranular, visual, parietal association, and auditory cortex. ROI for the cortex ranged about 150–180 coronal images depending on each sample. ROI for the hippocampus were placed in the CA1, CA2, CA3, and dentate gyrus and ranged about 60–80 coronal images. ROI for the rostral piriform cortex was placed only on one image that is at a level equivalent of figure 22 in the mouse brain atlas (Paxinos, 2001). ROI for the caudal piriform cortex and amygdala ranged from a level equivalent of figure 22 to figure 54 in Paxinos (2001), over about 24–38 coronal images. ROI for the amygdala includes the lateral amygdaloid nucleus (LA), basolateral amygdaloid nucleus, anterior part (BLA), amygdaloid nucleus, anterior part (MeA), and posterior nuclei.

Tractography.

Diffusion-weighted (DW) magnetic resonance images were acquired with P0 and E16 mouse brains immersed in fomblin oil, using a 16.4 Tesla Bruker scanner and a 10-mm birdcage quadrature coil. Three-dimensional DW spin-echo sequences were acquired using the following parameters: repetition time = 400 ms; echo time = 22.8 ms; imaging resolution, 0.08 × 0.08 × 0.08 mm and a signal average of 1. Each dataset was composed of 2 B_o and 30 direction DW images (b value of 5,000 s/mm^2, ∂/Δ = 2.5/14 ms).

Reconstruction and tractography were performed with Diffusion Toolkit (Ruopeng Wang and Van J. Wedeen. TrackVis.org, Martinos Center for Biomedical Imaging, Massachusetts General Hospital, Boston, MA) according to high angular resolution diffusion (HARDI) and Q-ball models (Moldrich et al. 2010; Tuch, 2004; Hess et al., 2006). HARDI/Qball modeling and modified FACT (Mori et al., 1999) tractography limits were set at fractional anisotropy (FA) values greater than 0.1 and turning angle ≤ 45°. Hand-drawn regions of interest (ROI) on color-coded fractional anistoropy (FA) maps were used to elicit the streamlines of interest using TrackVis (Ruopeng Wang and Van J. Wedeen. TrackVis.org, Martinos Center for Biomedical Imaging). The diffusion direction shown in the color-coded FA map is as follows: green, anterior-posterior; blue, dorsal-ventral; red, medial-lateral. Streamlines are shown as one color per ROI.

Tractography streamline number was retrieved from TrackVis and adjusted for region of interest volume. Mean ± s.e.m. values between *Fgfr3*$^{-/-}$ and wild type controls were compared for statistical differences using t-test (GraphPad Prism v.4), where significance was set at $P < 0.05$ and $n = 3$.

Histology and microscopy.

E18.5 brains were immersion fixed overnight in 4% (w/v) paraformaldehyde in PBS at 4°C, and processed for paraffin-sectioning. Serial sections at 10 μm were mounted on Polysine glass slides (Thermoscientific, Braunshweig, Germany). Sections were deparaffinised in Xylene and rehydrated in graded ethanol (100, 95, and 70%) and water. Sections were then immersed in 0.1% Cresyl Violet solution until adequate staining was achieved. After rinsing with tap water, sections were dehydrated and mounted using DPX mountant for microscopy (VWR International Ltd, England). A Zeiss Axioskop microscope (Carl Zeiss, Germany) was used for photography and the images were captured by Axiovision Release 4.7.1 software (Carl Zeiss Germany).

BrdU Labelling and Immunohistochemistry

Time-mated females were intraperitoneally injected with 50 μg/g body weight BrdU in PBS for 1 hr prior to sacrifice. Sections at rostral and caudal levels equivalent of plates 1 and 9, respectively (Jacobowitz and Abbott, 1997) were used. After rehydration, antigen retrieval was achieved by boiling in 10 mM citrate buffer (pH 6.4) for 30 min. Sections were incubated in 2 mol/dm^3 HCl for 1 hr at 37°C. Blocking solution was 10% (v/v) normal goat serum, 2% bovine albumin, 0.1% (v/v) Triton-X100 in PBS. Incubation with the anti-BrdU antibody (B-44, 1:75; BD Biosciences, Oxford, UK) was performed overnight at 4°C. The secondary antibody was applied for 2 hr. Antibodies used were: anti-GFAP (rabbit polyclonal, 1:200; DAKO); anti-Olig2 (rabbit polyclonal, 1:200; Abcam, Cambridge, UK), anti-NeuN (mouse monoclonal MAB377, 1:200; Chemicon, Nottingham, UK), anti-BrdU (rat polyclonal, 1:200; Abcam), anti-Tbr1 (rabbit polyclonal, 1:500; Abcam), anti-Tbr2 (rabbit polyclonal, 1:2,000; Chemicon, Nottingham, UK); anti-Pax6 (rabbit polyclonal, 1:500; Covance, Cambridge BioScience, Cambridge, UK); anti-GAD67 (mouse monoclonal, 1:500; Chemicon); goat anti-rat AlexaFluor568, goat anti-mouse AlexaFluor 488, and goat-anti-rabbit AlexaFluor 594 (1:200; Invitrogen, Paisley,

UK). Sections were mounted in VectaSield (VectorLabs, Burlingame, CA) containing 4′,6-diamidino-2-phenylindole (DAPI). Axioplan2 microscope and ISIS software (Carl Zeiss, Germany) was used for photography. Cell counts and counting area measurements were made using Adobe Photoshop. Morphology data were graphed using GraphPad Prism (v4.0). Statistical differences were calculated in GraphPad Prism using either a *t*-test or a two-way ANOVA with Dunnett's post-hoc *t*-test where the *P* value was set at 0.05.

Dye Tracing Studies

Brains from E14.5 and E18.5 from each genotype were examined. To label thalamic fibers at E14.5, single crystals of 1,19-dioctadecyl-3,3,39,39-tetramethylindocarbocyanine perchlorate (DiI) were placed in the dorsal thalamus. For topographical studies, single crystals of DiI and 4-(4-(dihexadecylamino) styryl)-N-methylpyridinium iodide (DiA) (Molecular Probes, Eugene, OR) were placed with a stainless steel electrode into the occipital (putative visual) and parietal (putative somatosensory) cerebral cortical areas, respectively, of both hemispheres of each brain. After injections, brains were kept in 2% paraformaldehyde for 2–3 weeks at room temperature in the dark. Brains were washed in PBS (0.1 M, pH 7.4), embedded into 4% agarose (Sigma, St. Louis, MO), and cut at 100 μm with a Vibroslicer (Leica, Wetzlar, Germany; VT1000S). Sections were counterstained with 0.5 μg/ml DAPI (49-6-diamidino-2-phenylindole), mounted in PBS/glycerol or AquaPolymount (Polysciences, Warrington, PA) onto slides, and analyzed using an epifluorescence microscope (Leica, DMR, or Zeiss).

ACKNOWLEDGMENTS

We thank colleagues and core facility staff of the Beatson Institute for Cancer Research for their continuous support and encouragement. We thank Noelia Garcia from GL-B laboratory for excellent technical assistance. Funding for this project was received from the Neuroscience Foundation, Glasgow (T.I.), the National Health and Medical Research Council (NHMRC) Australia project grant 631552 (L.J.R.), and Spanish Ministry of Science and Innovation BFU2009-08261 and CONSOLIDER CSD2007-00023 (G.L.-B.). R.X.M. was supported by a CJ Martin Fellowship and L.J.R. is supported by an NHMRC Principal Research Fellowship.

REFERENCES

Carney RS, Alfonso TB, Cohen D, Dai H, Nery S, Stoica B, Slotkin J, Bregman BS, Fishell G, Corbin JG. 2006. Cell migration along the lateral cortical stream to the developing basal telencephalic limbic system. J Neurosci 26: 11562–11574.

Cholfin JA, Rubenstein JL. 2008. Frontal cortex subdivision patterning is coordinately regulated by Fgf8, Fgf17, and Emx2. J Comp Neurol 509:144–155.

Colvin JS, Bohne BA, Harding GW, McEwen DG, Ornitz DM. 1996. Skeletal overgrowth and deafness in mice lacking fibroblast growth factor receptor 3. Nat Genet 12:390–397.

Deng C, Wynshaw-Boris A, Zhou F, Kuo A, Leder P. 1996. Fibroblast growth factor receptor 3 is a negative regulator of bone growth. Cell 84:911–921.

Dong HW, Petrovich GD, Swanson LW. 2001. Topography of projections from amygdala to bed nuclei of the stria terminalis. Brain Res Brain Res Rev 38: 192–246.

Englund C, Fink A, Lau C, Pham D, Daza RA, Bulfone A, Kowalczyk T, Hevner RF. 2005. Pax6, Tbr2, and Tbr1 are expressed sequentially by radial glia, intermediate progenitor cells, and postmitotic neurons in developing neocortex. J Neurosci 25:247–251.

Fukuchi-Shimogori T, Grove EA. 2003. Emx2 patterns the neocortex by regulating FGF positional signaling. Nat Neurosci 6:825–831.

Gutin G, Fernandes M, Palazzolo L, Paek H, Yu K, Ornitz DM, McConnell SK, Hebert JM. 2006. FGF signalling generates ventral telencephalic cells independently of SHH. Development 133: 2937–2946.

Hess CP, Mukherjee P, Han ET, Xu D, Vigneron DB. 2006. Q-ball reconstruction of multimodal fiber orientations using the spherical harmonic basis. Magn Reson Med 56:104–117.

Hevner RF, Shi L, Justice N, Hsueh Y-P, Sheng M, Smiga S, Bulfone A, Goffinet AM, Campagnoni AT, Rubenstein JLR. 2001. Tbr1 regulates differentiation of the preplate and layer 6. Neuron 29: 353–366.

Hirata T, Li P, Lanuza GM, Cocas LA, Huntsman MM, Corbin JG. 2009. Identification of distinct telencephalic progenitor pools for neuronal diversity in the amygdala. Nat Neurosci 12: 141–149.

Iwata T, Hevner RF. 2009. Fibroblast growth factor signaling in development of the cerebral cortex. Dev Growth Differ 51:299–323.

Jacobowitz DM, Abbott LC. 1997. Chemoarchitedtonic atlas of the developing mouse brain. Boca Raton, FL: CRC Press.

Kang W, Wong LC, Shi SH, Hebert JM. 2009. The transition from radial glial to intermediate progenitor cell is inhibited by FGF signaling during corticogenesis. J Neurosci 29:14571–14580.

Lopez-Bendito G, Molnar Z. 2003. Thalamocortical development: how are we going to get there? Nat Rev Neurosci 4: 276–289.

Mason I. 2007. Initiation to end point: the multiple roles of fibroblast growth factors in neural development. Nat Rev Neurosci 8:583–596.

Moldrich RX, Pannek K, Hoch R, Rubenstein JL, Kurniawan ND, Richards LJ. 2010. Comparative mouse brain tractography of diffusion magnetic resonance imaging. Neuroimage 51:1027–1036.

Mori S, Crain BJ, Chacko VP, van Zijl PC. 1999. Three-dimensional tracking of axonal projections in the brain by magnetic resonance imaging. Ann Neurol 45:265–269.

Ohkubo Y, Uchida AO, Shin D, Partanen J, Vaccarino FM. 2004. Fibroblast growth factor receptor 1 is required for the proliferation of hippocampal progenitor cells and for hippocampal growth in mouse. J Neurosci 24:6057–6069.

Paek H, Gutin G, Hebert JM. 2009. FGF signaling is strictly required to maintain early telencephalic precursor cell survival. Development 136:2457–2465.

Paxinos GFBJ. 2001. The mouse brain in stereotaxic coordinates. New York: Academic Press.

Pontious A, Kowalczyk T, Englund C, Hevner RF. 2008. Role of intermediate progenitor cells in cerebral cortex development. Dev Neurosci 30:24–32.

Rakic P, Ayoub AE, Breunig JJ, Dominguez MH. 2009. Decision by division: making cortical maps. Trends Neurosci 32:291–301.

Scearce-Levie K, Roberson ED, Gerstein H, Cholfin JA, Mandiyan VS, Shah NM, Rubenstein JL, Mucke L. 2008. Abnormal social behaviors in mice lacking Fgf17. Genes Brain Behav 7:344–354.

Smith KM, Ohkubo Y, Maragnoli ME, Rasin MR, Schwartz ML, Sestan N, Vaccarino FM. 2006. Midline radial glia translocation and corpus callosum formation require FGF signaling. Nat Neurosci 9:787–797.

Sturrock RR. 1978. Development of the indusium griseum. I. A quantitative light microscopic study of neurons and glia. J Anat 125:293–298.

Thomson RE, Pellicano F, Iwata T. 2007. Fibroblast growth factor receptor 3 kinase domain mutation increases cortical progenitor proliferation via mitogen-activated protein kinase activation. J Neurochem 100: 1565–1578.

Thomson RE, Kind PC, Graham NA, Etherson ML, Kennedy J, Fernandes

AC, Marques CS, Hevner RF, Iwata T. 2009. Fgf receptor 3 activation promotes selective growth and expansion of occipitotemporal cortex. Neural Dev 4:4.

Tole S, Gutin G, Bhatnagar L, Remedios R, Hebert JM. 2006. Development of midline cell types and commissural axon tracts requires Fgfr1 in the cerebrum. Dev Biol 289:141–151.

Tuch DS. 2004. Q-ball imaging. Magn Reson Med 52:1358–1372.

Turner N, Grose R. 2010. Fibroblast growth factor signalling: from development to cancer. Nat Rev Cancer 10: 116–129.

Tyszka JM, Readhead C, Bearer EL, Pautler RG, Jacobs RE. 2006. Statistical diffusion tensor histology reveals regional dysmyelination effects in the shiverer mouse mutant. Neuroimage 29:1058–1065.

Vaccarino FM, Grigorenko EL, Smith KM, Stevens HE. 2009. Regulation of cerebral cortical size and neuron number by fibroblast growth factors: implications for autism. J Autism Dev Disord. 39:511–520.

Developmental Dynamics